Cellulose (2016) 23:3001–3012
DOI 10.1007/s10570-016-1003-1

ORIGINAL PAPER

Rheological behavior of highly loaded cellulose nanocrystal/poly(vinyl alcohol) composite suspensions

Caitlin E. Meree · Gregory T. Schueneman · J. Carson Meredith · Meisha L. Shofner

Received: 21 January 2016 / Accepted: 1 July 2016 / Published online: 12 July 2016

Abstract Recent emphasis on the pilot scale production of cellulosic nanomaterials has increased interest in the effective use of these materials as reinforcements for polymer composites. An important, enabling step to realizing the potential of cellulosic nanomaterials in their applications is the materials processing of CNC/polymer composites through multiple routes, i.e. melt, solution, and aqueous processing methods. Therefore, the objective of this research is to characterize the viscoelastic behavior of aqueous nanocomposite suspensions containing cellulose nanocrystals (CNCs) and a water-soluble polymer, poly(vinyl alcohol) (PVA). Specifically, small amplitude oscillatory shear measurements were performed on neat PVA solutions and CNC-loaded PVA suspensions. The experimental results indicated that the methods used in this study were able to produce high-quality nanocomposite suspensions at high CNC loadings, up to 67 wt% with respect to PVA. Additionally, the structure achieved in the nanocomposite suspensions was understood through component attributes and interactions. At CNC loadings near and less than the percolation threshold, a polymer mediated CNC network was present. At loadings well above the percolation threshold, a CNC network was present, indicated by limited molecular weight dependence of the storage modulus. Overall, these results provide increased fundamental understanding of CNC/PVA suspensions that can be leveraged to develop advanced aqueous processing methods for these materials.

Keywords Poly(vinyl alcohol) · Cellulose nanocrystals · Rheology · Nanocomposite · Cellulose · Viscoelasticity

C. E. Meree · M. L. Shofner (✉)
School of Materials Science and Engineering, Georgia Institute of Technology, Atlanta, GA, USA
e-mail: meisha.shofner@mse.gatech.edu

C. E. Meree · J. C. Meredith · M. L. Shofner
Renewable Bioproducts Institute, Georgia Institute of Technology, Atlanta, GA, USA

G. T. Schueneman
Forest Products Laboratory, U.S. Forest Service, Madison, WI, USA

J. C. Meredith
School of Chemical and Biomolecular Engineering, Georgia Institute of Technology, Atlanta, GA, USA

Introduction

Cellulose nanocrystals (CNCs) are nanoscale fibers derived from cellulose structures found in plant sources such as wood, hemp, cotton, and linen (Postek et al. 2011) as well as organisms such as bacteria, tunicate, and algae (Khalil et al. 2012; Moon et al. 2011; Ramires and Dufresne 2011). Depending on the cellulose source material, CNCs (Lahiji et al. 2010)

have widths between 3 and 50 nm and lengths over a greater range, from 50 nm to greater than 1 μm (Abitbol et al. 2011; Beck-Candanedo et al. 2005; Dong and Gray 1997; Moon et al. 2011). Based on the theoretical mechanical properties of crystalline cellulose, the strength and modulus of CNCs are expected to be high, approximately 7.5 GPa (Reising et al. 2012) and 100–220 GPa (Hossain et al. 2012; Lahiji et al. 2010; Moon et al. 2011; Reising et al. 2012; Silverio et al. 2013; Wu et al. 2013), respectively. Combining these anticipated mechanical properties (Abitbol et al. 2011) with their relatively low density and their potential to be produced from renewable sources makes them an attractive filler for polymer composites.

Many CNCs are hydrophilic and can form stable suspensions in water. Therefore, they do not have a high level of inherent compatibility with many widely used polymers in their native state. Their hydrophilic nature has led to studies of CNC composites with water-soluble matrices such as poly(vinyl alcohol) (PVA) (Abitbol et al. 2011; Fortunati et al. 2013; Frone et al. 2011; Mihranyan 2013; Pakzad et al. 2012a, b; Peresin et al. 2010; Roohani et al. 2008; Silverio et al. 2013; Uddin et al. 2011a, b; Yang et al. 2013). PVA is a synthetically-derived, flexible, water-soluble, biodegradable, and non-toxic polymer (Gao et al. 2010; Kim et al. 2004; Lyoo et al. 2006; Song and Kim 2004) as well as the most widely produced synthetically derived water-soluble polymer (Roohani et al. 2008). It is most commonly synthesized from a poly(vinyl acetate) precursor via free-radical polymerization in the presence of alcohol. PVA is used in a variety of industries including the medical, packaging, and food industry as well as paper manufacturing (Chiellini et al. 2003; Jiang et al. 2011; Lyoo et al. 2006; Ram and Mandal 2004). Additionally, chemically cross-linked PVA is used as a membrane in fuel cells, waste water treatment (Bolto et al. 2009) and tissue scaffolding (Scholten et al. 2011) due to its barrier properties against oxygen and aromatic compounds as well as its resistance to many solvents and oils (Huang et al. 2010; Maiti et al. 2012; Pakzad et al. 2012a; Wang and Hsieh 2010). It has also been used in for biomedical applications such as tissue mimicking, cell culturing, and vascular implants (Jiang et al. 2011).

Based on the wide application spectrum of PVA and the hydrophilic nature of CNCs, CNC/PVA nanocomposites present a potentially sustainable option for materials development and design in the nanocomposite field as these nanocomposites are predicted to be light-weight, biocompatible, and biodegradable materials. Beyond CNCs, research has been conducted on cellulose/PVA composites and nanocellulose/PVA composites for a multitude of applications. In terms of mechanical properties, tensile strength and modulus was seen to increase by about 13 and 34 %, respectively with the addition of 3 wt% microfibrillated cellulose into a neat PVA matrix (Tanpichai et al. 2014). In addition, the incorporation of bleached softwood Kraft microfibers (MF) to a PVA matrix has resulted a doubling of tensile strength and 2.5 times increase in stiffness with only 5 wt% loading (Chakraborty et al. 2006). Measurement of the dynamic viscoelastic properties of microcrystalline cellulose/PVA composites showed storage and loss modulus values on the order of 10 kPa, appropriate for orthopedic applications (Mihranyan 2013). The addition of microfibrillated cellulose (MFC) to a PVA matrix has resulted in an increase in storage modulus above the glass transition temperature (Lu et al. 2008) as well as increased thermal stability (Qiu and Netravali 2012) due to the slightly increased degradation onset temperature. Bacterial cellulose (BC), a type of CNC, has also been added to PVA hydrogels to form nanocomposites with mechanical and morphological properties suitable for the replacement of cardiovascular tissue (Millon and Wan 2006). Specifically, mechanical tests indicated that BC/PVA hydrogels could be formulated to closely mimic the anisotropic properties of the native tissue. Though these cellulose and nanocellulose fillers show property improvements when combined with PVA, CNCs are believed to be beneficial as structural fillers compared to other cellulosic particles due to their highly ordered and rigid nature opposed to the large disordered regions present in MFs and MFCs. For example, while neat PVA shows light transmittance of almost 92 % at 500 nm wavelengths, neat cellulose nanofiber mats have very low light transmittance around 7 %. Through the addition of cellulose nanofibers to PVA, composite films have been shown to have excellent light transmittance at loadings up to 70 % cellulose nanofiber with transmittance over 80 % in the wavelength range of 500–800 nm (Tang and Liu 2008). Additionally, wood-derived CNCs are available in pilot scale quantities, unlike other types of CNCs,

which allows for them to be studied more effectively as fillers in polymer composites.

An important, enabling step to producing CNC/PVA composites is the materials processing. Since both components have an affinity for water, the processing may be accomplished through methods which use an aqueous medium. Thus, an understanding of the rheological properties of the nanocomposite suspension is needed to logically process these materials and describe their interactions and structure; however, the rheological properties of CNC/PVA systems have been only briefly discussed in the literature and center around physically bonded cyrogels produced though multiple freeze and thaw cycles. Freeze/thaw cycles are of interest as they provide a mechanism for producing porous polymer matrices with a three-dimensional support system capable of optical and tissue engineering applications. Through the freeze/thaw method, stable PVA composite sponges can be formulated though hydrogen bonds serving as physical crosslinks (Wang et al. 2010). Fibrous cellulose powder/PVA composites subjected to freeze and thaw cycles with CNC/PVA weight per weight ratios of 75/25, 50/50, and 25/75 displayed solid-like behavior due to the high loadings of CNCs (Chang et al. 2008). Additionally, physically crosslinked freeze/thaw gels were also seen to exhibit rigid character with high elasticity after CNC loading (Mihranyan 2013). In a separate study, significantly increased storage modulus with CNC loading in PVA/starch freeze/thaw nanocomposite sponges was observed and attributed to increased hydrogen bonding between the hydrophilic matrix and fillers as well as compaction of the polymer chains and CNCs during freeze/thaw cycles (Wang et al. 2010). To compliment these studies, the aim of this research is to more fully understand the effect of CNCs on the rheological behavior of PVA in a physically crosslinked gel system without freeze and thaw cycles which may be more applicable to large scale processing of these materials with high CNC loadings and a wider range of applications.

Methods and procedures

PVA polymers purchased from Sigma Aldrich with weight average molecular weights of 31,000–50,000 g mol^{-1} (98–99 % hydrolyzed), 85,000–124,000 g mol^{-1} (99+ % hydrolyzed), and 146,000–186,000 g mol^{-1} (99+ % hydrolyzed) were used as received. The CNCs used in this work were provided by the USDA Forest Products Laboratory and received in aqueous suspension. The suspension had a 5.5 wt% solids loading. Similar wood-derived CNCs used by the authors had an average length of 138 ± 22 nm and average diameter of 6.4 ± 0.6 nm (Xu et al. 2013), resulting in aspect ratios between approximately 16 and 27. In all nanocomposite suspensions produced, deionized water was used as the solvent.

Neat PVA solutions and CNC/PVA nanocomposite suspensions were prepared for rheological study by heating deionized water to boiling using a hot plate and adding PVA in quantities to produce solutions with solids loadings of 15 wt%. The PVA solutions were then stirred in a covered beaker for 1 h using a Talboy overhead mixer model 134-1 at 1900 RPM with a 5 cm diameter stainless steel propeller blade. Nanocomposite suspensions were prepared by adding the desired amount of CNCs to the previously prepared PVA solutions at a temperature of 100 °C. The CNCs were incorporated by stirring with the same overhead mixer at 1900 RPM for 90 min. During stirring, the nanocomposite suspensions were left uncovered to allow excess water to evaporate to obtain a final overall solids loading of 15 wt%. Samples were made with all three PVA polymers.

After sample preparation, the CNC/PVA samples were further treated using a centrifuge at a rotational speed of 3000 RPM for 30 min to remove any visible bubbles present after mixing. The solids loadings of the neat PVA solutions and nanocomposite suspensions were confirmed using thermogravimetric analysis (TGA) with a TA Instruments Q5000IR TGA. Experiments were conducted in a nitrogen environment at a gas flow rate of 20 mL min^{-1}. A nominal sample mass of 20 mg was tested by heating the samples from room temperature to 120 °C at 10 °C min^{-1} followed by an isothermal step at 120 °C for 20 min. The solids loading was calculated using the sample weight remaining at the end of the isothermal step. Polarized light microscopy was conducted to examine the morphology of each sample. PVA solutions and nanocomposite suspensions were cast onto glass slides and examined via polarized microscopy using an Olympus BX51 optical microscope and 530 nm red wave plate. Additionally, images were taken using a 8 megapixel mobile phone

camera (Motorola Droid Razr HD) to assess optical clarity.

The sample nomenclature used in this paper is of the general form WXY-Z where W indicates the polymer molecular weight (L for 31,000–50,000 g mol^{-1}, M for 85,000–124,000 g mol^{-1}, and H for 146,000–186,000 g mol^{-1}), X indicates if the sample is a neat PVA solution (N) or nanocomposite suspension (C), Y gives the PVA loading in weight percent, and Z gives the CNC loading in weight percent. For example, the nanocomposite suspension with the 31,000–50,000 g mol^{-1} PVA polymer, a PVA loading of 10 wt% and a CNC solids loading of 5 wt% is denoted as LC10-5. A listing of the samples prepared and characterized in this work is given in Table 1.

Rheological experiments were performed using a TA Instruments AR2000EX rheometer with a 25 mm parallel plate fixture at 25 °C. After sample loading, the gap was set to 1000 μm, and a thin coating of silicone oil (Acros Organics) with viscosity of 150 mPa s was applied to the exposed sample surface using a pipette to reduce water evaporation during testing. Steady shear and small amplitude oscillatory shear tests were performed. Steady shear tests were performed following a pre-shear step at 1 s^{-1}. Data were collected from low to high shear rates. These tests were conducted at times points of 1, 3, and 5 days after sample preparation to determine if any changes in solution structure due to aging were occurring. Apparent viscosity values obtained from the steady shear tests were corrected using the instrument software to obtain the true viscosity data shown here. Small amplitude oscillatory shear tests were performed using the same rheometer at a strain of 1 % following a pre-shear step at 1 s^{-1}. This strain was in the linear viscoelastic region as determined from strain sweep measurements at 100 rad/s. Each test was also conducted at time points of 1, 3, and 5 day after sample preparation to determine the effect of aging on dynamic behavior. Both steady shear and small amplitude oscillatory shear tests were conducted on neat polymer solutions while only small angle oscillatory shear tests was conducted on nanocomposite suspensions. With the exception of the neat 85 K sample at 3 days of aging, all tests were conducted at least twice with new samples used for each test. Error bars shown represent the spread in the experimentally measured values.

Results and discussion

Polarized light microscopy images of a neat CNC suspension, a neat PVA solution, and nanocomposite suspensions are shown in Fig. 1. In these images, isotropic regions appeared red or pink while anisotropic regions appeared blue or yellow (Abitbol et al. 2011). As shown in Fig. 1a, b, the neat CNC and neat PVA samples appeared largely isotropic. Figure 1c, d show anisotropic regions in the CNC/PVA

Table 1 Neat PVA solutions and nanocomposite suspensions used

PVA molecular weight (g mol^{-1})	Sample name	CNC/PVA	CNC wt% w.r.t. PVA
31,000–50,000	LN15-0	0	0
	LC12-3	0.25	20
	LC10-5	0.5	33
	LC7.5-7.5	1	50
	LC5-10	2	67
85,000–124,000	MN15-0	0	0
	MC12-3	0.25	20
	MC10-5	0.5	33
	MC7.5-7.5	1	50
	MC5-10	2	67
146,000–186,000	HN15-0	0	0
	HC12-3	0.25	20
	HC10-5	0.5	33
	HC7.5-7.5	1	50
	HC5-10	2	67

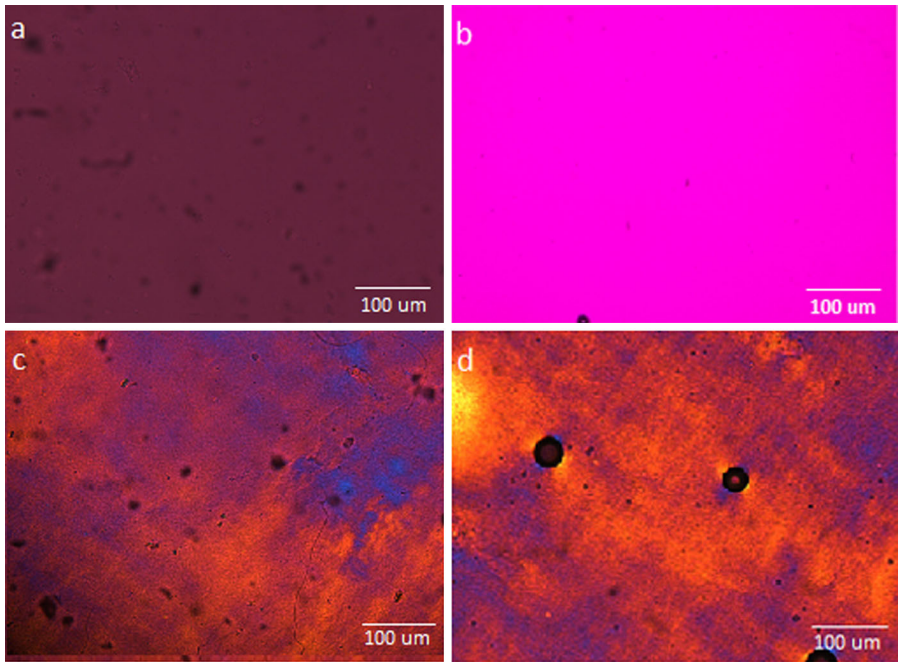

Fig. 1 Polarized light microscopy images of suspensions used for study: **a** Neat CNC suspension at 5.5 wt%, **b** Neat MN15-0, **c** MC10-5, **d** MC7.5-7.5

nanocomposite suspensions. In previous work by the authors with CNC/waterborne epoxy composites (Xu et al. 2013), aggregated CNCs appeared as discrete, birefringent regions when observed with polarized optical microscopy. Since no such features were observed here, the CNC dispersion was assumed to be homogeneous at this length scale, though CNC aggregation at smaller length scales cannot be ruled out.

The neat PVA solutions were characterized using steady shear rheological measurements at aging times of 1, 3, and 5 days. These data for the LN15-0, MN15-0, and HN15-0 are shown in Fig. 2. The LN15-0 sample showed the least amount of shear thinning of the three samples as well as limited change in the viscosity at aging times beyond 1 day. The MN15-0 and HN15-0 samples showed slight shear thinning behavior as well as increased aging behavior from 1 to 5 days indicated by the increase in the magnitude of the viscosity. This increase in viscosity with molecular weight was attributed to the networks that were formed in PVA solutions. These structures formed via two mechanisms: hydrogen bonding between hydroxyl groups of PVA and water and crystallite formation between PVA chains.

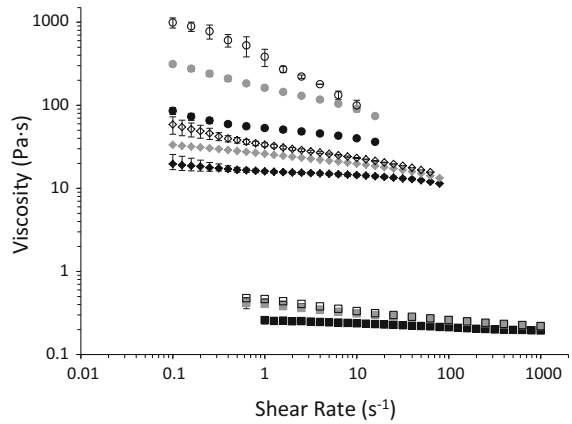

Fig. 2 Shear viscosity data for LN15-0 (*square*), MN15-0 (*diamond*), and HN15-0 (*circle*) at 1 day (*black*), 3 day (*gray*), and 5 day (*open*) aging points. Little aging behavior was seen at the lowest molecular weight while more significant aging was seen at the higher molecular weights as well as more significant shear thinning behavior at high shear rates

Crystallites formed when at least two PVA chains aligned over several PVA molecular segments. These segments interacted through hydrogen bonding and van der Waals forces, forming aqueous crystalline regions (Pritchard 1970). As the molecular weight of

the PVA increased, crystallite formation, elasticity, and viscosity also increased. The degree of crystallinity provided by these junctions in aged PVA solutions is typically low, less than 5 % for PVA solutions with similar solids loading when measured with X-ray scattering experiments (Holloway et al. 2013). Further increases in crystallinity can be achieved through the use of freeze–thaw cycles (Ricciardi et al. 2004), but that approach was not used in this research.

The viscosity increase with aging time for the LN15-0 sample at a shear rate of 1 s^{-1} from 1 to 5 days was approximately 80 % while the corresponding viscosity increase for the HN15-0 sample was 620 %. These trends were expected and attributed to differences in entanglement density and network formation for the different molecular weights studied here. The rate of aging also generally decreased as aging time increased. The decrease in aging rate in the latter portion of the aging cycle was attributed to increased compaction of the chains during the first stage of aging as junction points between polymer chains formed.

The shear thinning character of these solutions was described by fitting the viscosity data to a power law given by the equation below:

$$\eta(\dot{\gamma}) = m\dot{\gamma}^{n-1} \quad (1)$$

where $\eta(\dot{\gamma})$ is the viscosity as a function of shear rate, m is the consistency index, $\dot{\gamma}$ is the shear rate, and n is the power law exponent. The values of m and n were adjustable parameters in the fitting, and the value of n was used to understand the shear thinning character of the solutions. If n was equal to 1, the viscosity was constant with shear rate, indicating Newtonian behavior, and when n was less than 1, the viscosity decreased with increasing shear rate, indicating that the material was shear thinning. Smaller n values indicated a greater degree of shear thinning. The values for n and m for neat solutions as a function of aging time are given in Fig. 3. Generally, the value of n decreased with aging, indicating increased shear thinning character with increased aging times for the neat PVA solutions. The value of m increased with aging, consistent with network changes leading to increased viscosity.

When CNCs were added to the polymer solutions, the rheological behavior changed dramatically. As a result of increased elasticity in the nanocomposite suspensions, steady shear viscosity measurements could not be performed on these samples. Small angle oscillatory shear measurements of complex viscosity (η^*), storage modulus (G') and loss modulus (G'') were used instead to characterize the viscoelastic behavior of the nanocomposite suspensions and the CNCs' contribution to these properties. For comparison, the rheological properties of the neat PVA solutions were measured again using small angle oscillatory shear testing. The trends in complex viscosity as a function of angular frequency were similar to the trends in viscosity as a function of shear rate for the neat PVA samples. Specifically, the value of the complex viscosity was found to vary more with angular frequency as the aging time and PVA molecular weight increased. Due to the almost negligible elasticity of the LN15-0 samples, small angle oscillatory shear data were not able to be collected for this sample.

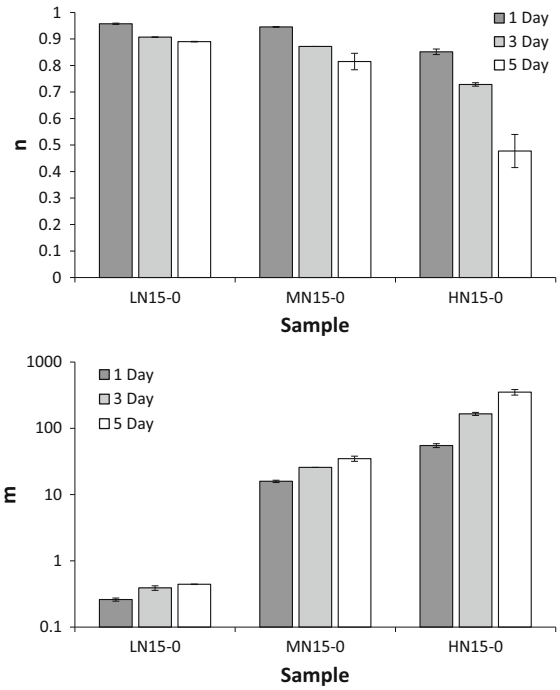

Fig. 3 Values of power law exponent (n) and consistency index (m) for neat PVA solutions

The first noticeable effect of CNC addition was seen in the mitigation of aging behavior due to the increased rigidity of the system with respect to the neat polymer solutions. As shown in Fig. 4, the value of η^* changed less with aging time in the nanocomposite

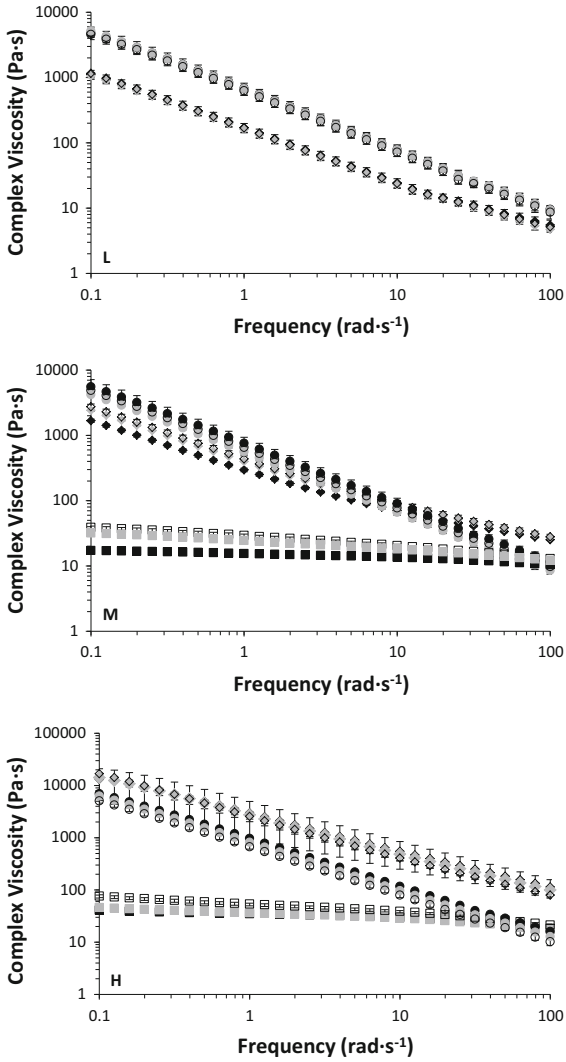

Fig. 4 Aging behavior of neat and nanocomposite suspensions at 1 day (*black*), 3 days (*gray*), and 5 days (*open*) for neat (*square*), C12-3 (*diamond*) and C5-10 (*circle*). *Top* (L samples). *Middle* (M samples). *Bottom* (H samples)

suspensions than in the neat PVA solutions. Interactions due to hydrogen bonding between CNCs and the PVA as well as between CNCs restricted polymer chain mobility and hindered increased polymer chain entanglement, likely leading to less structural change in the suspension with aging time. Conversely in the neat PVA systems, the chains were free to rotate, entangle, and form crystalline network junctions with one another over time due to physical bonding between the water molecules and the PVA chains (Gao et al. 2010). The aging trends were assumed to be largely related to changes in the polymer's ability to form physical bonds since previous work concerning the aging of neat CNC suspensions did not show substantial aggregation at storage times up to 375 days (Beck and Bouchard 2014).

To understand this behavior more fully, a modified power law based on η^* was applied to the data:

$$\eta^*(\omega) = m^*\omega^{n^*-1} \tag{2}$$

where $\eta^*(\omega)$ is the complex viscosity as a function of angular frequency, m^* is the consistency index and n^* is the power law exponent for complex viscosity. Figure 5 shows the value of n^* as a function of aging time for HN and HC samples. These results were representative of the three PVA molecular weights studied here. While distinct aging was seen in neat polymer solution, the structure of the nanocomposite suspensions changed less with increasing time, shown by lesser changes in the value of n^* as compared to the neat PVA solutions. As CNC loading increased in the suspension, the value of n^* from 1 to 5 days of aging time became nearly constant, indicating limited aging.

Analysis of the dynamic moduli data also led to insights into the effect of adding CNCs to the PVA suspensions. Figure 6 shows the dynamic moduli data, G' and G'', obtained for MN15-0 (neat PVA solution) and MC12-3 (nanocomposite suspension). An important difference was seen between these samples. For MN15-0, the value of G'' was greater than the value of G' for the range of frequencies measured, indicating the sample was a concentrated solution and not a gel. For the nanocomposite suspension shown (MC12-3), the value of G' was greater than the value of G'' over the range of frequencies measured indicating gelation

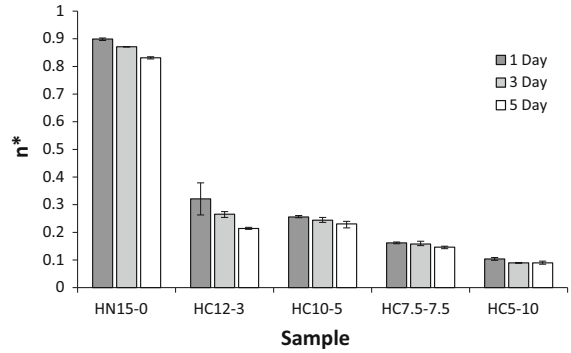

Fig. 5 CNC contribution to sample aging shown with the complex viscosity power law exponent (n^*). Overall, the addition of CNCs reduced aging in the suspensions

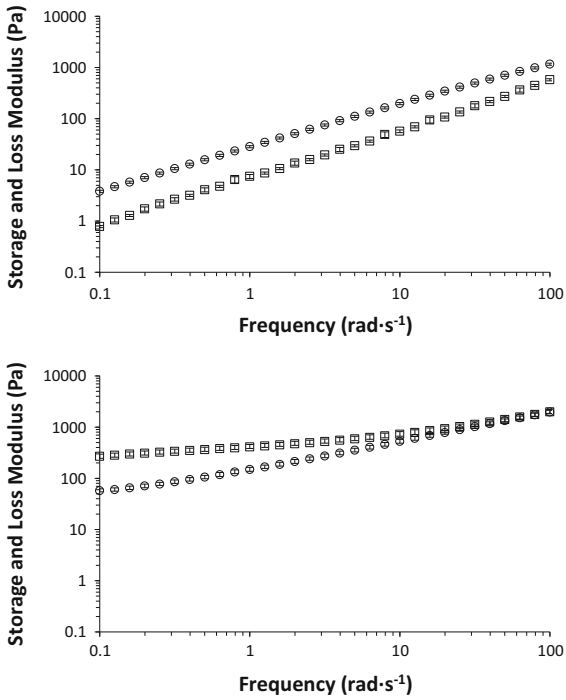

Fig. 6 Storage modulus and loss modulus for neat PVA and PVA/CNC suspension. The *top plot* shows the data for MN15-0 while the *bottom plot* shows the data for MC12-3. Storage modulus is denoted with (*open square*) while loss modulus is denoted with (*open circle*)

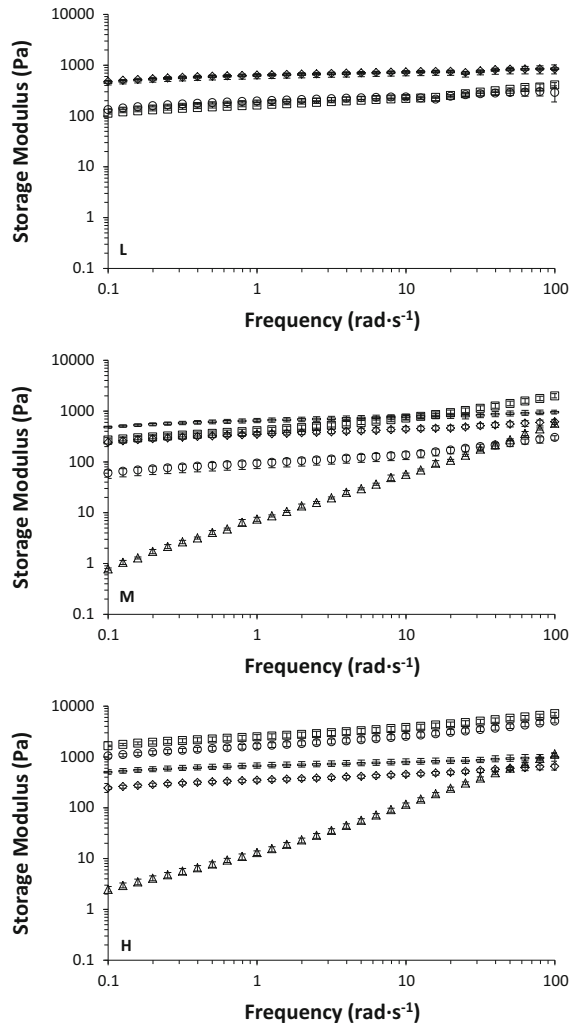

Fig. 7 Storage modulus data for neat and nanocomposite suspensions at 5 days aging time. Top: L samples. Middle: M samples. Bottom: H samples. N15-0 (*triangle*), C12-3 (*square*), C 10-5 (*circle*), C7.5-7.5 (*diamond*), and C5-10 (*dash*)

had occurred. Additionally, the frequency dependence of G' and G'' was weaker in the nanocomposite suspension, suggesting that an elastic network was formed in the suspension. All other nanocomposite suspensions showed similar trends in G' and G'', and the frequency dependence of G' and G'' continued to weaken with increasing CNC loading, shown for G' in Fig. 7.

The values of G' for neat solutions and nanocomposite suspensions are shown for all three PVA molecular weights in Fig. 7. From these data, two different trends were seen, and they were related to the polymer molecular weight and CNC loading. First, the trends observed for G' at lower CNC loadings were dependent on the polymer molecular weight. For the L molecular weight samples, G' increased with increasing CNC loading as the CNCs; however, the H molecular weight samples saw a decrease in G' with increasing CNC loading. The M molecular weight samples showed trends intermediate to the L and H molecular weight samples. The trends observed for the three molecular weights were attributed to differences in the nature of the neat polymer solutions. For the LN15-0 solution, the rheological characterization indicated that this solution behaved similarly to a Newtonian fluid with little shear rate dependence of the viscosity. This description was further supported by the inability to perform a small angle oscillatory shear experiment on the sample. Conversely, the MN15-0 and HN15-0 solutions showed more elastic character though their behavior was still more liquid-like than solid-like. Therefore, the addition of CNCs to

these solutions affected the value of G' differently because the neat PVA solutions at these molecular weights were structured differently, i.e. CNCs were able to more effectively reinforce the solutions that were more liquid-like in character and had a more complicated effect of solutions with more significant elasticity. Second, the value of G' at higher CNC loadings was similar for nanocomposite suspensions made with different polymer molecular weights. Since the values of G' at higher CNC loading showed little dependence on polymer molecular weight, this result suggested that the rheological response was related more strongly to the structuring of CNCs in the suspensions than any polymer or CNC-polymer networks present at the highest loadings used in this work.

In order to quantify the relative changes in the data with increasing CNC content and polymer molecular weight, the power law model presented earlier was adapted again for use with the G' data for the neat polymer solutions and the CNC nanocomposite suspensions from Fig. 7. This power law scaling of G' has been used with other concentrated polymer solution to understand network structure in PVA solutions (Kjøniksen and Nyström 1996). The results are shown in Fig. 8. The modified expression is shown below:

$$G'(\omega) = m'\omega^{n'} \tag{3}$$

where $G'(\omega)$ is the storage modulus as a function of angular frequency, m' is the consistency index, and n' is the modified power law exponent storage modulus behavior. The value of n' gave an indication of the differences in network behavior with lower values of n' corresponding to a more rigid network in the sample. As shown in Fig. 8, the value of n' decreased with increasing CNC content. At high CNC loadings, the value of n' was between 0.07 and 0.09 for nanocomposite suspensions made with all three molecular weights, suggesting that the CNC networks in the nanocomposite suspensions were structured similarly at these loadings. To more fully understand the network structures present in the samples, the storage modulus data obtained from the lowest testing frequency, 0.1 rad s^{-1}, are shown in Fig. 9. Again, a molecular weight dependent response was observed at lower CNC loadings, and a molecular weight independent response was observed at higher CNC loadings. These results further suggested that different types of networks were present in the samples as the CNC loading was changing and that the network was structured similarly at the highest CNC loading.

Considering these data together, rheological characterization of the neat PVA solutions and nanocomposite suspensions provided insight into the dynamics and structure of the materials. Aging processes were impacted by the addition of CNCs. Specifically, the addition of CNCs reduced aging, suggesting that the driving forces for phase separation between the PVA and water were kinetically suppressed. In the neat PVA solutions, aging occurred as junctions between individual polymer chains formed over time leading to microscale phase separation between the PVA and water (te Nijenhuis 1997). These connections, either in the form of polymer entanglements or microscale crystalline junctions, increased the viscosity of the solution and its elasticity (Pritchard 1970; te Nijenhuis 1997). CNCs appeared to impede the aging process by

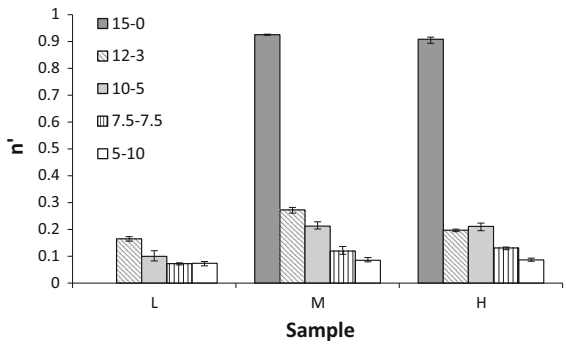

Fig. 8 Power law exponent (n') from storage modulus data

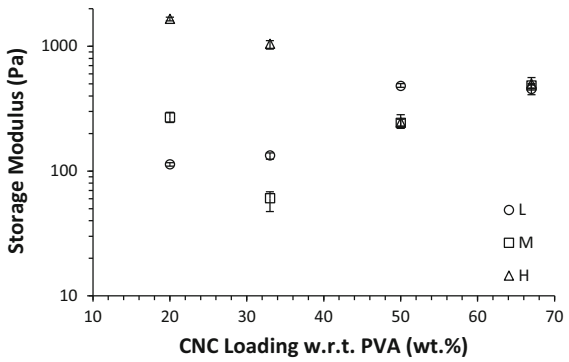

Fig. 9 Storage modulus values at a testing frequency of 0.1 rad s^{-1} for each molecular weight. Data collected at 5 days of aging were used. The data converged to a similar value at the highest CNC loading for all PVA molecular weights used in this work

physically interacting with the PVA and reducing its ability to form polymer junctions. All of the CNC concentrations used here were high enough to suppress these aging processes over the time scale of observation, leading to the need to understand more fully their structuring in the nanocomposite suspensions.

With regard to structure, the data obtained suggested that for the CNC loadings studied in this paper, networks were present in all of the nanocomposite suspensions. Network formation was indicated by the solid-like behavior of the nanocomposite suspensions, i.e. G' was generally greater than G'' at all frequencies used in the tests (data not shown). Conversely, the neat PVA solutions at each molecular weight appeared to be more liquid-like, though junctions between polymer chains in the form of entanglements or small crystallites would have been present (Pritchard 1970; te Nijenhuis 1997). Network formation dramatically increased the viscosity and elasticity of the suspensions with respect to the neat PVA solutions as would be expected. However, trends in G' data indicated that the type of network present in the sample was dependent on the CNC loading. For nanocomposite suspensions with PVA–CNC compositions of 12–3 and 10–5, the rheological response suggested that the network present in the material was composed of CNC and PVA with the polymer chains or their entanglements connecting CNCs. The stiffness of these polymer mediated junctions was directly related to the molecular weight of the polymer, as indicated by the values of G'. Specifically, the values of G' generally decreased with increasing CNC concentration for nanocomposite suspensions made with the H polymer, whereas the opposite trend was observed for nanocomposite suspensions made with the L polymer. These trends indicated that as the polymer molecular weight increased the polymer mediated CNC network became more robust. For nanocomposite suspensions with PVA–CNC compositions of 7.5-7.5 and 5-10, the rheological behavior suggested a network composed primarily of CNC with polymer mediated junctions playing a lesser role. This network structure was indicated by similar values of G' in the samples made with all three polymer molecular weights. The stiffness of this network was in some cases less than that of the polymer mediated CNC network, suggesting that entanglements and/or crystalline junctions present in the H and M samples were stiffer than CNC–CNC interactions. Overall, these trends indicated that more effective reinforcement was attained for lower molecular weight polymers; however at appropriate CNC concentrations, polymer mediated junctions can synergistically stiffen the nanocomposite gel.

This transition between network types approximately corresponded to the CNC percolation threshold. The percolation threshold was estimated using CNC aspect ratios between 15 and 30. These values were used since they correspond to dimensional data reported for similar wood-based CNCs used by the authors previously (Xu et al. 2013). Using this aspect ratio range, the percolation threshold was estimated to be between CNC volume fractions of 0.023–0.047. The percolation threshold values were calculated as 0.7 divided by the CNC aspect ratio (Favier et al. 1997). For the nanocomposite suspensions studied here, the volume fractions for PVA–CNC loadings of 12–3, 10–5, 7.5–7.5, and 5–10 were 0.019, 0.031, 0.048, and 0.064, respectively. Therefore, polymer mediated networks played a greater role in determining the rheological response at CNC loadings slightly below or near the percolation threshold, and CNC networks determined the rheological response at CNC loadings well above the percolation threshold.

Conclusion

Neat PVA and CNC/PVA nanocomposite suspensions were studied to provide insight into water-based processing of these materials at high CNC loadings. The results of these experiments indicated that CNC/PVA suspensions with loadings of up to 67 wt% CNC with respect to PVA could be produced via relatively simple water-based solution processing methods. Using rheological characterization, elements of the structure of the CNC/PVA suspensions were inferred. Specifically, these data suggested that two types of networks were present in these materials, polymer mediated CNC networks at lower CNC loadings and CNC networks at higher CNC loadings, and the transition between these networks was related to the CNC percolation threshold. Using these results, it is envisioned that nanocomposite suspensions containing physically bonded networks may be processed in similar methods to polymer melts, ultimately leading to more scalable processing strategies for these materials. This topic is the focus of continuing

research by the authors and will be reported in a subsequent publication.

Acknowledgments The authors thank the Renewable Bioproducts Institute for providing a Paper Science and Engineering Fellowship for C.E.M as well as support for the purchase of some of the materials and supplies used in this work. The authors also thank the USDA Forest Service Forest Products Laboratory for providing the CNCs used in this work.

Compliance with ethical standards

Conflict of interest The authors declare that they have no conflict of interest.

References

Abitbol T, Johnstone T, Quinn TM, Gray DG (2011) Reinforcement with cellulose nanocrystals of poly(vinyl alcohol) hydrogels prepared by cyclic freezing and thawing. Soft Matter 7:2373–2379. doi:10.1039/c0sm01172j

Beck S, Bouchard J (2014) Effect of storage conditions on cellulose nanocrystal stability. Tappi J 13:53–61

Beck-Candanedo S, Roman M, Gray DG (2005) Effect of reaction conditions on the properties and behavior of wood cellulose nanocrystal suspensions. Biomacromolecules 6:1048–1054. doi:10.1021/bm049300p

Bolto B, Tran T, Hoang M, Xie ZL (2009) Crosslinked poly(-vinyl alcohol) membranes. Prog Polym Sci 34:969–981. doi:10.1016/j.progpolymsci.2009.05.003

Chakraborty A, Sain M, Kortschot M (2006) Reinforcing potential of wood pulp-derived microfibres in a PVA matrix. Holzforschung 60:53–58. doi:10.1515/hf.2006.010

Chang CY, Lue A, Zhang L (2008) Effects of crosslinking methods on structure and properties of cellulose/PVA hydrogels Macromol. Chem Phys 209:1266–1273. doi:10.1002/macp.200800161

Chiellini E, Corti A, D'Antone S, Solaro R (2003) Biodegradation of poly (vinyl alcohol) based materials. Prog Polym Sci 28:963–1014. doi:10.1016/s0079-6700(02)00149-1

Dong XM, Gray DG (1997) Induced circular dichroism of isotropic and magnetically-oriented chiral nematic suspensions of cellulose crystallites. Langmuir 13:3029–3034. doi:10.1021/la9610462

Favier V, Dendievel R, Canova G, Cavaille JY, Gilormini P (1997) Simulation and modeling of three-dimensional percolating structures: case of a latex matrix reinforced by a network of cellulose fibers. Acta Mater 45:1557–1565. doi:10.1016/S1359-6454(96)00264-9

Fortunati E, Puglia D, Monti M, Santulli C, Maniruzzaman M, Kenny JM (2013) Cellulose nanocrystals extracted from okra fibers in PVA nanocomposites. J Appl Polym Sci 128:3220–3230. doi:10.1002/app.38524

Frone AN, Panaitescu DM, Donescu D, Spataru CI, Radovici C, Trusca R, Somoghi R (2011) Preparation and characterization of PVA composites with cellulose nanofibers obtained by ultrasonication. BioResources 6:487–512

Gao HW, Yang RJ, He JY, Yang L (2010) Rheological behaviors of PVA/H_2O solutions of high-polymer. J Appl Polym Sci 116:1459–1466. doi:10.1002/app.31677

Holloway JL, Lowman AM, Palmese GR (2013) The role of crystallization and phase separation in the formation of physically cross-linked PVA hydrogels. Soft Matter 9:826–833. doi:10.1039/c2sm26763b

Hossain KMZ, Jasmani L, Ahmed I, Parsons AJ, Scotchford CA, Thielemans W, Rudd CD (2012) High cellulose nanowhisker content composites through cellosize bonding. Soft Matter 8:12099–12110. doi:10.1039/c2sm26912k

Huang CC, Lou CW, Lu CT, Huang SH, Chao CY, Lin JH, Lee JH (2010) Evaluation of the preparation and biocompatibility of poly(vinyl alcohol)(PVA)/chitosan composite electrospun membranes. Multi-functional materials and structures III, Pts 1 and 2, vol 123–125. Advanced materials research. Trans Tech Publications Ltd, Stafa-Zurich, pp 975–978. doi:10.4028/www.scientific.net/AMR.123-125.975

Jiang S, Liu S, Feng WH (2011) PVA hydrogel properties for biomedical application. J Mech Behav Biomed Mater 4:1228–1233. doi:10.1016/j.jmbbm.2011.04.005

Khalil H, Bhat AH, Yusra AFI (2012) Green composites from sustainable cellulose nanofibrils: a review. Carbohydr Polym 87:963–979. doi:10.1016/j.carbpol.2011.08.078

Kim SS, Seo IS, Yeum JH, Ji BC, Kim JH, Kwak JW, Yoon WS, Noh SK, Lyoo WS (2004) Rheological properties of water solutions of syndiotactic poly(vinyl alcohol) of different molecular weights. J Appl Polym Sci 92:1426–1431. doi:10.1002/app.13685

Kjøniksen A-L, Nyström B (1996) Effects of polymer concentration and cross-linking density on rheology of chemically cross-linked poly(vinyl alcohol) near the gelation threshold. Macromolecules 29:5215–5222. doi:10.1021/ma960094q

Lahiji RR, Xu X, Reifenberger R, Raman A, Rudie A, Moon RJ (2010) Atomic force microscopy characterization of cellulose nanocrystals. Langmuir 26:4480–4488. doi:10.1021/la903111j

Lu J, Wang T, Drzal LT (2008) Preparation and properties of microfibrillated cellulose polyvinyl alcohol composite materials. Compos Part A-Appl S 39:738–746. doi:10.1016/j.compositesa.2008.02.003

Lyoo WS, Yeum JH, Kwon OW, Shin DS, Han SS, Kim BC, Jeon HY, Noh SK (2006) Rheological properties of high molecular weight (HMW) syndiotactic poly(vinyl alcohol) (PVA)/HMW atactic PVA blend solutions. J Appl Polym Sci 102:3934–3939. doi:10.1002/app.24223

Maiti J, Kakati N, Lee SH, Jee SH, Viswanathan B, Yoon YS (2012) Where do poly(vinyl alcohol) based membranes stand in relation to Nafion® for direct methanol fuel cell applications? J Power Sources 216:48–66. doi:10.1016/j.jpowsour.2012.05.057

Mihranyan A (2013) Viscoelastic properties of cross-linked polyvinyl alcohol and surface-oxidized cellulose whisker hydrogels. Cellulose 20:1369–1376. doi:10.1007/s10570-013-9882-x

Millon LE, Wan WK (2006) The polyvinyl alcohol-bacterial cellulose system as a new nanocomposite for biomedical applications. J Biomed Mater Res B 79B:245–253. doi:10.1002/jbm.b.30535

Moon RJ, Martini A, Nairn J, Simonsen J, Youngblood J (2011) Cellulose nanomaterials review: structure, properties and nanocomposites. Chem Soc Rev 40:3941–3994. doi:10.1039/c0cs00108b

Pakzad A, Simonsen J, Yassar RS (2012a) Elastic properties of thin poly(vinyl alcohol)-cellulose nanocrystal membranes. Nanotechnology. doi:10.1088/0957-4484/23/8/085706

Pakzad A, Simonsen J, Yassar RS (2012b) Gradient of nanomechanical properties in the interphase of cellulose nanocrystal composites. Compos Sci Technol 72:314–319. doi:10.1016/j.compscitech.2011.11.020

Peresin MS, Habibi Y, Zoppe JO, Pawlak JJ, Rojas OJ (2010) Nanofiber composites of polyvinyl alcohol and cellulose nanocrystals: manufacture and characterization. Biomacromolecules 11:674–681. doi:10.1021/bm901254n

Postek MT, Vladar A, Dagata J, Farkas N, Ming B, Wagner R, Raman A, Moon RJ, Sabo R, Wegner TH, Beecher J (2011) Development of the metrology and imaging of cellulose nanocrystals. Meas Sci Technol 22:1–10. doi:10.1088/0957-0233/22/2/024005

Pritchard JG (1970) Poly(vinyl alcohol): basic properties and uses. Gordon and Breach Science Publishers, New York

Qiu KY, Netravali AN (2012) Fabrication and characterization of biodegradable composites based on microfibrillated cellulose and polyvinyl alcohol. Compos Sci Technol 72:1588–1594. doi:10.1016/j.compscitech.2012.06.010

Ram S, Mandal TK (2004) Photoluminescence in small isotactic, atactic and syndiotactic PVA polymer molecules in water. Chem Phys 303:121–128. doi:10.1016/j.chemphys.2004.05.006

Ramires EC, Dufresne A (2011) A review of cellulose nanocrystals and nanocomposites. Tappi J 10:9–16

Reising AB, Moon RJ, Youngblood JP (2012) Effect of particle alignment on mechanical properties of neat cellulose nanocrystal films. J For 2:32–41

Ricciardi R, Auriemma F, Gaillet C, De Rosa C, Lauprêtre F (2004) Investigation of the crystallinity of freeze/thaw poly(vinyl alcohol) hydrogels by different techniques. Macromolecules 37:9510–9516. doi:10.1021/ma048418v

Roohani M, Habibi Y, Belgacem NM, Ebrahim G, Karimi AN, Dufresne A (2008) Cellulose whiskers reinforced polyvinyl alcohol copolymers nanocomposites. Eur Polym J 44:2489–2498. doi:10.1016/j.eurpolymj.2008.05.024

Scholten PM, Ng KW, Joh K, Serino LP, Warren RF, Torzilli PA, Maher SA (2011) A semi-degradable composite scaffold for articular cartilage defects. J Biomed Mater Res A 97A:8–15. doi:10.1002/jbm.a.33005

Silverio HA, Neto WPF, Pasquini D (2013) Effect of incorporating cellulose nanocrystals from corncob on the tensile, thermal and barrier properties of poly(vinyl alcohol) nanocomposites. J Nanomater. doi:10.1155/2013/289641

Song SI, Kim BC (2004) Characteristic rheological features of PVA solutions in water-containing solvents with different hydration states. Polymer 45:2381–2386. doi:10.1016/j.polymer.2004.01.057

Tang CY, Liu HQ (2008) Cellulose nanofiber reinforced poly(vinyl alcohol) composite film with high visible light transmittance. Compos Part A Appl S 39:1638–1643. doi:10.1016/j.compositesa.2008.07.005

Tanpichai S, Sampson WW, Eichhorn SJ (2014) Stress transfer in microfibrillated cellulose reinforced poly(vinyl alcohol) composites. Compos Part A Appl S 65:186–191. doi:10.1016/j.compositesa.2014.06.014

te Nijenhuis K (1997) Thermoreversible networks: viscoelastic properties and structure of gels. Advances in polymer science, vol 130. Springer, Berlin

Uddin AJ, Araki J, Gotoh Y (2011a) Characterization of the poly(vinyl alcohol)/cellulose whisker gel spun fibers. Compos Part A Appl S 42:741–747. doi:10.1016/j.compositesa.2011.02.012

Uddin AJ, Araki J, Gotoh Y (2011b) Toward "strong" green nanocomposites: polyvinyl alcohol reinforced with extremely oriented cellulose whiskers. Biomacromolecules 12:617–624. doi:10.1021/bm101280f

Wang YH, Hsieh YL (2010) Crosslinking of polyvinyl alcohol (PVA) fibrous membranes with glutaraldehyde and PEG diacylchloride. J Appl Polym Sci 116:3249–3255. doi:10.1002/app.31750

Wang YX, Chang CY, Zhang LN (2010) Effects of freezing/thawing cycles and cellulose nanowhiskers on structure and properties of biocompatible starch/PVA sponges. Macromol Mater Eng 295:137–145. doi:10.1002/mame.200900212

Wu XW, Moon RJ, Martini A (2013) Crystalline cellulose elastic modulus predicted by atomistic models of uniform deformation and nanoscale indentation. Cellulose 20:43–55. doi:10.1007/s10570-012-9823-0

Xu SH, Girouard N, Schueneman G, Shofner ML, Meredith JC (2013) Mechanical and thermal properties of waterborne epoxy composites containing cellulose nanocrystals. Polymer 54:6589–6598. doi:10.1016/j.polymer.2013.10.011

Yang J, Han CR, Duan JF, Xu F, Sun RC (2013) Mechanical and viscoelastic properties of cellulose nanocrystals reinforced poly(ethylene glycol) nanocomposite hydrogels. ACS Appl Mater Interfaces 5:3199–3207. doi:10.1021/am4001997